



# Responses of the Pacific and Atlantic decadal variabilities under global warming by using CMIP6 models

Yuyang Shang<sup>1</sup> · Peng Liu<sup>2</sup> · Sheng Wu<sup>3</sup>

Received: 20 October 2022 / Accepted: 19 November 2023 / Published online: 5 December 2023  
© The Author(s) 2023

## Abstract

Decadal variability in the ocean is an important indicator of climate system shifts and has considerable influences on marine ecosystems. We investigate the responses of decadal variability over the global ocean regions using nine CMIP6 models (BCC-CSM2-MR, CESM2-WACCM, CMCC-ESM2, EC-Earth3-Veg-LR, FGOAL-f3-L, INM-CM5-0, MIROC6, MPI-ESM1-2-LR, and NorESM2-MM). Our results show that climate models can capture the Pacific Decadal Oscillation, Tropical Pacific Decadal Variability, South Pacific Decadal Oscillation, and Atlantic Multidecadal Variability under present-day conditions. The ocean decadal variabilities are becoming weaker and their periods are decreasing, especially under the strong global warming scenario. However, there is a discrepancy between the Tropical Pacific Decadal Variability and the other three modes of climate variability. This might be caused by the nearly unchanged atmospheric forcing in the equatorial region, which is decreasing in the higher latitude regions.

**Keywords** Decadal variability · Global warming · CMIP6

## 1 Introduction

In recent years, ocean decadal variability has attracted ever-increasing attention for its importance in modulating global warming (England et al. 2014; Bordbar et al. 2017). In its sixth assessment report (AR6), the Intergovernmental Panel on Climate Change (IPCC) clearly affirmed the significant

contribution of human activity to the warming of the atmosphere, oceans, and land by increasing carbon dioxide (CO<sub>2</sub>) emissions since the Industrial Revolution (Li 2022; Thapliyal et al. 2023). However, the increase in global mean surface temperature (GMST) is not linear but instead has two alternating phases, which include accelerated warming and a global warming hiatus (IPCC, 2013). GMST increased rapidly during 1920–1945 and 1977–2000 but stalled during 1946–1976 and 2001–2013 (England et al. 2014, 2015; Bordbar et al. 2019). The common view is that greenhouse gases and anthropogenic aerosols dominate long-term warming trends, while natural internal variability determines the climate system phase shift (Farneti 2017). By conducting the pacemaker experiments, it was suggested that the global warming hiatus may be caused by the negative phase of the Pacific Decadal Oscillation (PDO) and Atlantic Multidecadal Variability (AMV) (Kosaka and Xie 2013; McGregor et al. 2014; Deser et al. 2017). This indicates that decadal climate variability should be taken into account for near-term climate predictions (Hawkins and Sutton 2009; Liu 2012).

Ocean decadal variability is not only significant for global low-frequency variability but also plays a key role in extreme weather and climate events along ocean coasts (Alexander 2010; Deser et al. 2010; Di Lorenzo et al. 2023). Ocean

---

Responsible Editor: Richard John Greatbatch

✉ Sheng Wu  
wishwishwish@pku.edu.cn

Yuyang Shang  
wfsy2007@163.com

Peng Liu  
liupeng2020@ouc.edu.cn

<sup>1</sup> Beijing Institute of Metrology, No.12, Anyuan Dongli Block 1, Chaoyang District, Beijing 100029, China

<sup>2</sup> Frontiers Science Center for Deep Ocean Multispheres and Earth System, Key Lab of Submarine Geosciences and Prospecting Techniques, MOE and College of Marine Geosciences, Ocean University of China, Qingdao 266100, China

<sup>3</sup> Laboratory for Climate and Ocean-Atmosphere Studies, Department of Atmospheric and Oceanic Sciences, School of Physics, Peking University, Beijing 100871, China

decadal variability has been identified as a leading driver of changes in some marine extreme events (Roemmich and McGowan 1995; Mantua et al. 1997; Hare et al. 1999), such as marine heatwaves (Di Lorenzo and Mantua 2016; Holbrook et al. 2019) and tropical storms (Chu and Clark 1999; Li et al. 2015). Based on observational data, many indices have been defined to evaluate the Pacific decadal variability, such as PDO (Mantua et al. 1997), the North Pacific Gyre Oscillation (NPGO; Di Lorenzo et al. 2008), the Interdecadal Pacific Oscillation (IPO; Power et al. 1999), South Pacific Decadal Oscillation (SPDO; Hsu and Chen 2011), and Tropical Pacific Decadal Variability (TPDV; Liu and Di Lorenzo 2018). The AMV index is derived as the latitude-weighted average of the North Atlantic low-passed filtered sea surface temperature (SST) anomaly field. Previous studies have shown that decadal variability has a shortening period and weakening amplitude in the northern high-latitude regions under global warming (Fang et al. 2014; Cheng et al. 2016; Wu and Liu 2020). They speculate that the response of decadal variability is associated with the acceleration of the ocean Rossby wave (Wu et al. 2018; Li et al. 2020). Other works imply that atmospheric stochastic forcing may be the dominant forcing for decadal variability (Clement et al. 2015; Wu and Liu 2020). However, the responses and mechanisms of decadal variability in the tropical and southern hemispheres remain unclear. Different global warming scenarios predicted in the AR6, which are based on different anthropogenic emission pathways, might indicate various ocean decadal variabilities with different impacts on the ocean system. In this research, we attempt to show the responses of decadal variability in different ocean basins to different warming scenarios.

The outline of the paper is managed as follows. Section 2 describes the dataset and methods used in this study. Section 3 includes the ocean decadal variability derived from observations, provided as a reference in Section 3.1, and presents the modeled responses of ocean decadal variability to global warming in Section 3.2. Section 4 presents the conclusion and discusses the mechanisms.

## 2 Data and methods

### 2.1 Observational data

This study employs observational data as benchmarks to outline the current ocean decadal variability. The data used here are monthly mean sea surface temperature SST (unit, °C) values extracted from the Extended Reconstructed Sea Surface Temperature Dataset (ERSST) provided by the National Oceanic and Atmospheric Administration (NOAA) (Huang et al. 2017). The dataset is organized in a  $2 \times 2$  spatial grid, covering the period from 1854 onward. Due to the sparse data in the early years, high biases persisted until the 1870s.

After the 1920s, the SST bias dropped to very low levels due to ship-based observations (Huang et al. 2015). The dataset used in this study is ERSSTv4, which extends from 1900 to 2016 and is further interpolated at a resolution of  $3.75 \times 3.75$ . ERSSTv4 has significant improvements compared with the previous versions (Smith et al. 2008), in representation of global warming. It has a stronger globally averaged warming trend and could better reflect El Niño/La Niña (Huang et al. 2015; Liu et al. 2015) and the PDO (Huang et al. 2017).

### 2.2 CMIP6 output

The results of nine model simulations are chosen from the World Climate Research Programme's (WCRP) Coupled Model Intercomparison Project 6 (CMIP6) dataset. These models, including BCC-CSM2-MR, CESM2-WACCM, CMCC-ESM2, EC-Earth3-Veg-LR, FGOAL-f3-L, INM-CM5-0, MIROC6, MPI-ESM1-2-LR, and NorESM2-MM are from different institutions and countries (Table. 1). This study uses the preindustrial (PI) run as the control run; the historical (HIS) and four shared socioeconomic pathways (SSP1-2.6, SSP2-4.5, SSP3-7.0, SSP5-8.5) are taken as the different global warming experiments. The radiative forcing will increase by 2.6, 4.5, 7.0, and 8.5 W/m<sup>2</sup> relative to the present-day conditions under SSP1-2.6, SSP2-4.5, SSP3-7.0, and SSP5-8.5, respectively (O'Neill et al. 2016). All PI simulations in the CMIP6 model selected here are longer than 500 years. HIS simulations cover the period from 1850 to 2014, and SSP runs contain the period from the year 2015 to 2100, as shown in Table 1.

### 2.3 Statistical methods

We first interpolate observation data onto a grid of  $3.75 \times 3.75$  as a benchmark, derive the annual averaged SST from the simulated monthly model results, and calculate the SST anomaly (SSTA) pattern by subtracting the climatological mean from the annual averaged values at each grid point. We then calculate the low-pass filtered data twice using a 3-year running mean for the global region (Zhang et al. 1997). To remove the trend caused by anthropogenic emissions, we remove the linear tendency within the ERSSTv4 and HIS runs and then use the empirical mode decomposition (EMD) method to remove trends in the SSP runs (Cheng et al. 2016; Wu et al. 2022). EMD uses the characteristic time scale to identify intrinsic oscillatory modes contained in the signal. It can continuously extract the components of each scale that make up the original signal from high frequency to low frequency; thus, the last component can represent the global warming trend (Flandrin et al. 2004; Wu and Liu 2020).

We separate the Pacific and Atlantic into four regions, i.e., the North Pacific (NP, 110° E–100° W, 20° N–60° N),

**Table 1** CMIP6 models used in this study

	Model	Institution	Country	Horizontal resolution	Pre-industrial runs (year)	Historical runs (year)	SSP runs (year)
1	BCC-CSM2-MR	BCC (Beijing Climate Center)	China	360×232	1850–2449	1850–2014	2015–2100
2	CESM2-WACCM	NCAR (National Center for Atmospheric Research)	USA	320×384	0001–0499	1850–2014	2015–2100
3	CMCC-ESM2	CMCC (Euromediterranean Center on Climate Change)	Italia	362×292	1850–2349	1850–2014	2015–2100
4	EC-Earth3-Veg-LR	EC-Earth-Consortium	Europe	362×292	2300–2800	1850–2014	2015–2100
5	FGOALS-f3-L	CAS (Chinese Academy of Sciences)	China	360×218	0600–1099	1850–2014	2015–2100
6	INM-CM5-0	INM (Marchuk Institute of Numerical Mathematics of the Russian Academy of Sciences)	Russia	720×720	1996–3196	1850–2014	2015–2100
7	MIROC6	MIROC	Japan	360×256	3200–3999	1850–2014	2015–2100
8	MPI-ESM1-2-LR	MPI-M (Max Planck Institute for Meteorology)	Germany	256×220	1850–2849	1850–2014	2015–2100
9	NorESM2-MM	NCC (supported by the Research Council of Norway)	Norway	360×384	1200–1699	1850–2014	2015–2100

the Tropical Pacific (TP, 110° E–100° W, 10° S–10° N), the South Pacific (SP, 110° E–100° W, 60° S–20° S), and the North Atlantic (NA, 80° W–0°, 0–70° N). The PDO, TPDV, and SPDO indices are derived as the principal components of the leading empirical orthogonal function (EOF) mode of the low-passed SSTA data over the NP, TP, and SP, respectively. Meanwhile, the AMV index is calculated by the area-averaged low-passed SSTA over the NA (Enfield et al. 2001). Then the above indices are normalized by the corresponding standard deviations (Wu et al. 2018), and global SSTA fields are regressed on the normalized indices to obtain the decadal variability patterns.

After obtaining decadal variability patterns and time series, we calculate the power spectra and standard deviation (STD) to analyze the change in decadal variabilities' periods and amplitudes. The multimodel mean value is obtained based on the results of spectral analyses applied to each model. The regional average STD was also calculated for all four ocean regions described above.

### 3 Results

#### 3.1 Ocean decadal variability

The regression coefficients of the PDO, TPDV, and SPDO show an El Niño Southern Oscillation (ENSO)-like pattern, and the AMV is characterized by a basin-scale pattern (Fig. 1a–d). For instance, the PDO can be modeled to

a simple integration of the Aleutian Low variability (1st EOF mode of the sea level pressure anomaly). Moreover, the dynamic adjustment of heat content anomalies in the tropics and the teleconnection between tropical and extra-tropical regions are important to the PDO (Newman et al. 2016; Ding et al. 2013). Furthermore, the SP also exhibits obvious decadal fluctuations with weaker intensity than that in the NP (Fig. 1a–c). Similar to the PDO, the SPDO integrates the atmospheric forcing from the local and tropical teleconnections (Shakun and Shaman 2009). The tropics seem to play a role in synchronizing the NP and SP (Liu and Di Lorenzo 2018); therefore, the low-passed SSTA is used to discuss the tropical decadal variability below. The maximum regression amplitude of the TPDV is located in the tropics, which shows a clear link between the ENSO and the TPDV (Fig. 1b). However, it is still unclear whether the TPDV arose from ENSO events or teleconnection from extra-tropical or local atmospheric forcing. The typical AMV basin-scale pattern (Deser and Blackmon 1993; Kushnir 1994) (Fig. 1d) can be shaped by only the atmospheric forcing (Clement et al. 2015), while Zhang et al. (2016) argue for the potential opposite effect of the atmospheric signal according to fully coupled model simulations. Some previous works show clear evidence for the linkage between AMV and Atlantic Meridional Overturning Circulation (AMOC). For instance, a stronger AMOC would lead to a warmer subpolar gyre and a colder recirculation gyre (Joyce and Zhang 2010; Zhang et al. 2019).

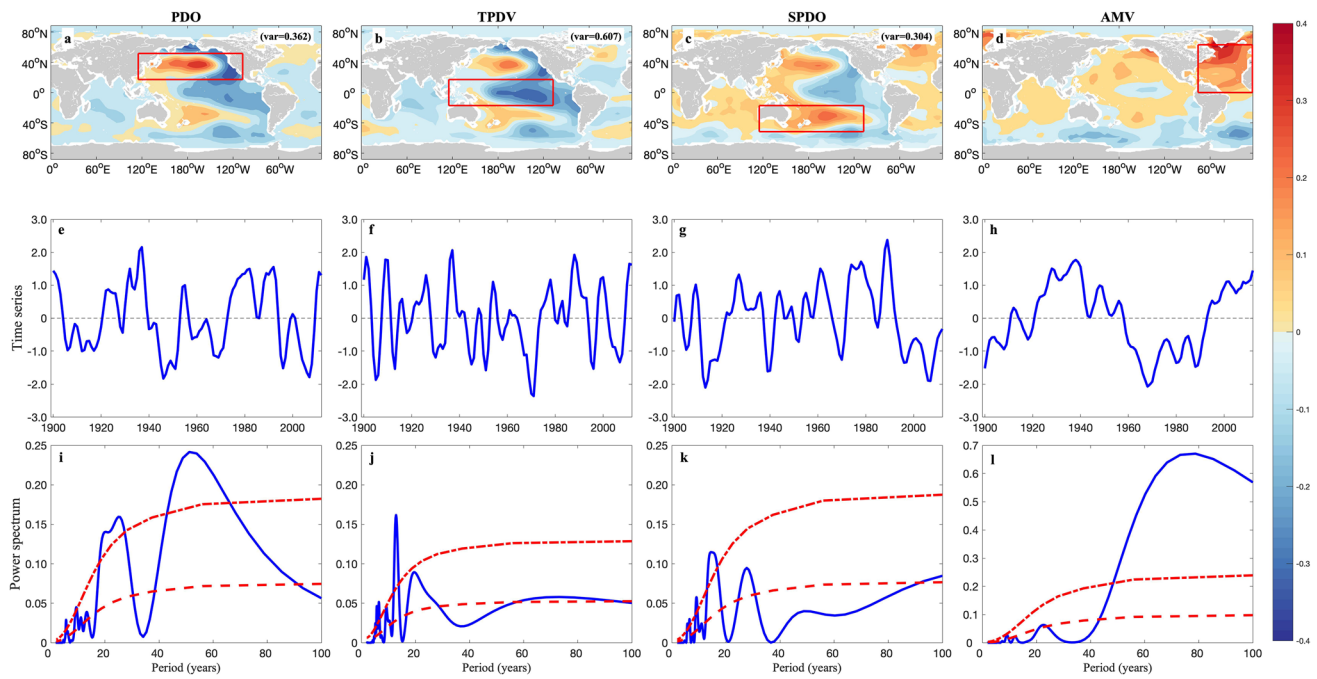


**Fig. 1** Observed (top) spatial regression pattern, (middle) time series, and (bottom) power spectrum for **a**, **e**, and **i** PDO; **b**, **f**, and **j** TPDV; **c**, **g**, and **k** SPDO; and **d**, **h**, and **l** AMV indices (1900–2016). A 3-year running mean twice was applied to the local SST (each grid point) over the North Pacific (110° E–100° W, 20° N–60° N), Tropical Pacific (110° E–100° W, 10° S–10° N), South Pacific (110°

E–100° W, 60° S–20° S) and North Atlantic (80° W–0°, 0°–70° N). And the PDO, TPDV, SPDO, and AMV indices were calculated prior to computing the regression. The dashed line and dash-dotted line in the bottom row represent 90 and 50% confidence intervals, respectively, calculated by the Monte Carlo method

The indices of ocean decadal variability are shown in Fig. 1e–h with the power spectrum of the PDO, TPDV, SPDO, and AMV indices (Fig. 1i–l). The three peaks in the PDO power spectrum over the 90% confidence interval are calculated by the Monte Carlo method over the same length with ERSSTv4. The peaks in the power spectrum indicate the periods of 25 and 50 years, respectively (Fig. 1i). Two peaks have also been identified in the power spectrum of SPDO analysis (Fig. 1k). However, the 45-year peak only passes 50% confidence interval, as the shorter period (15–25 years) crosses the 90% confidence threshold. The power of the TPDV at 90% confidence has an obvious peak at approximately 15 years, which corresponds to a bi-decadal periodicity but lacks a multidecadal signal. In contrast, the AMV shows a stronger power at approximately 70 years and no significant signal at less than 50 years (Fig. 1l). This multidecadal variability can easily be seen from the AMV index (Fig. 1h). It is worth mentioning that there is low confidence for multidecadal variability cause the data length.

### 3.2 Responses to global warming

We then compare the CMIP6 coupled climate model simulations (Table 1) with the observational data. The average of HIS of the nine models reasonably reproduces the spatial

patterns of the PDO, TPDV, SPDO, and AMV (b panels in Figs. S1–S4). However, subtle differences still exist between the models and observations, as explained below. The regression coefficients are smaller in the models, especially for the PDO and SPDO patterns in the tropics and the TPDV pattern in the NP and SP. In the NP, the maximum regressing coefficient is located in the Kuroshio–Oyashio Extension region (Fig. S1b) while that is seated in the central North Pacific in observation (Fig. 1d). In the TP, the observed maximum is located in the Niño 3.4 region (Fig. 1b), but it presents in the model simulations as a narrow region along the equator (Fig. S2b). Under different global warming scenarios (SSP runs), the ocean decadal variability shares a similar pattern, but all become weaker, implying the weakening of amplitude (Figs. S1–S4). Figure 2 shows this comparison in the form of a Taylor diagram (Taylor 2001), which indicates that the root mean square (RMS) differences between ERSSTv4, and the nine model members are small (green dashed line). Each circle point in Fig. 2 represents a member of the CMIP6 model, and the pink star indicates the ERSSTv4 values. Although climate models can reproduce similar patterns of ocean decadal variability, the correlation coefficients are quite low. In PDO, TPDV, and SPDO, only 37, 52, and 20% of members have correlation coefficients higher than 0.8. No member is higher than 0.7 for the AMV, which is comparable to the

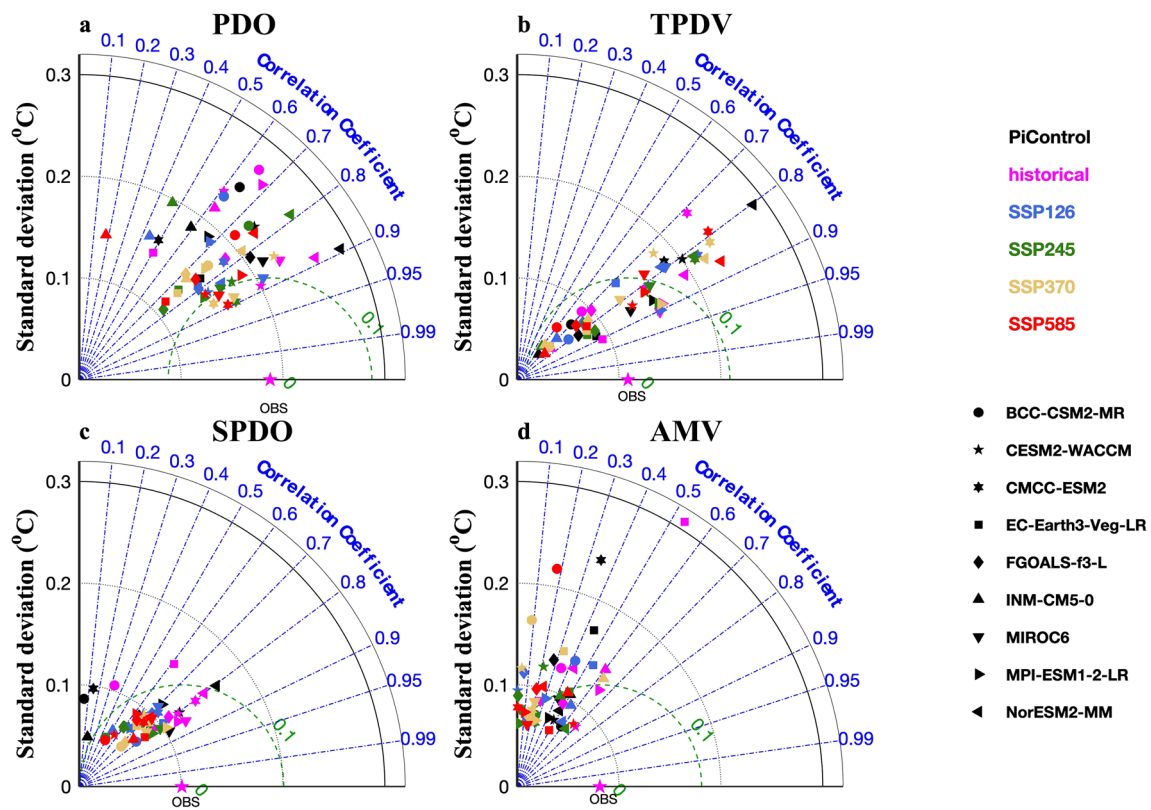


**Fig. 2** Taylor diagrams of **a** PDO, **b** TPDV, **c** SPDO, and **d** AMV. Pink pentagram represents ERSSTv4. Black, pink, blue, green, yellow, and red dots represent PI, HIS, SSP1-2.6, SSP2-4.5, SSP3-7.0, and SSP5-8.5 of nine CMIP6 models, respectively. In this diagram, the distance of a point from the origin is its standard deviation (°C)

and the distance from the reference point (pink pentagram, ERSSTv4) is the root-mean-square error (RMSE) between the pattern and the reference pattern. The increment in the pattern correlation coefficient is not linear (0–0.9–0.95–0.99)

results obtained by using the leading EOF mode as the AMV index Fig. S5). This implies that the models do not actually appear to reproduce the observed ocean decadal variability, especially in NA. With stronger global warming scenarios (comparison between blue and red circles), the STD decreases in all decadal variabilities, which is consistent with the change in the pattern.

To quantify the weakening of ocean decadal variability, we calculate the STD of the SSTA field over the global ocean (Fig. S6) and the amplitude of the response in four regions (NP, TP, SP, and NA) (Fig. 3). According to the multimodel average (black line in Fig. 3), the decadal variability of the four modes has a significant downward trend. In the mid and high latitudes (NP, SP, and NA), an obvious drop from HIS to SSP126 has been identified compared to the relatively small deviations observed from PI to HIS (Fig. 3a, c, and d). Nevertheless, the weakening trend of the TPDV in the tropic region is mild between different climate background scenarios (Fig. 3b), which means that the sensitivity of the SST variability might be weaker in lower latitude regions. A previous study found that the tropical decadal variations

appear largely random under global warming (Ding et al. 2019). However, some models, such as NorESM2-MM and MIROC6, show more distinct variations in the TP, which might be relevant to the higher weight in the temperature calculation (Song et al. 2022). On the other hand, the ranges of the NP, SP, and NA are small in each scenario, but the range is larger in the TP, which shows that the model difference is much greater in the tropics. In the NP and NA (Fig. 3a and d), the strength of the decadal variability is reduced from 0.39/0.36 in the PI to 0.25/0.23 in the SSP5-8.5 run, which is almost a 40% reduction. The SP has the largest decrease (46%), and the TP has the smallest decrease (30%). Overall, the weakening of ocean decadal variability is substantial in the four different regions and is much higher at high latitudes.

Under global warming, ocean decadal variability shows a tendency for shorter periods. The multimodel means of the PDO, TPDV, SPDO, and AMV power spectra for the PI, HIS, SSP1-2.6, SSP2-4.5, SSP3-7.0, and SSP5-8.5 are shown in Fig. 4, and the main periods are shown in Table 2. To diminish the impact of the specific model, we use nine

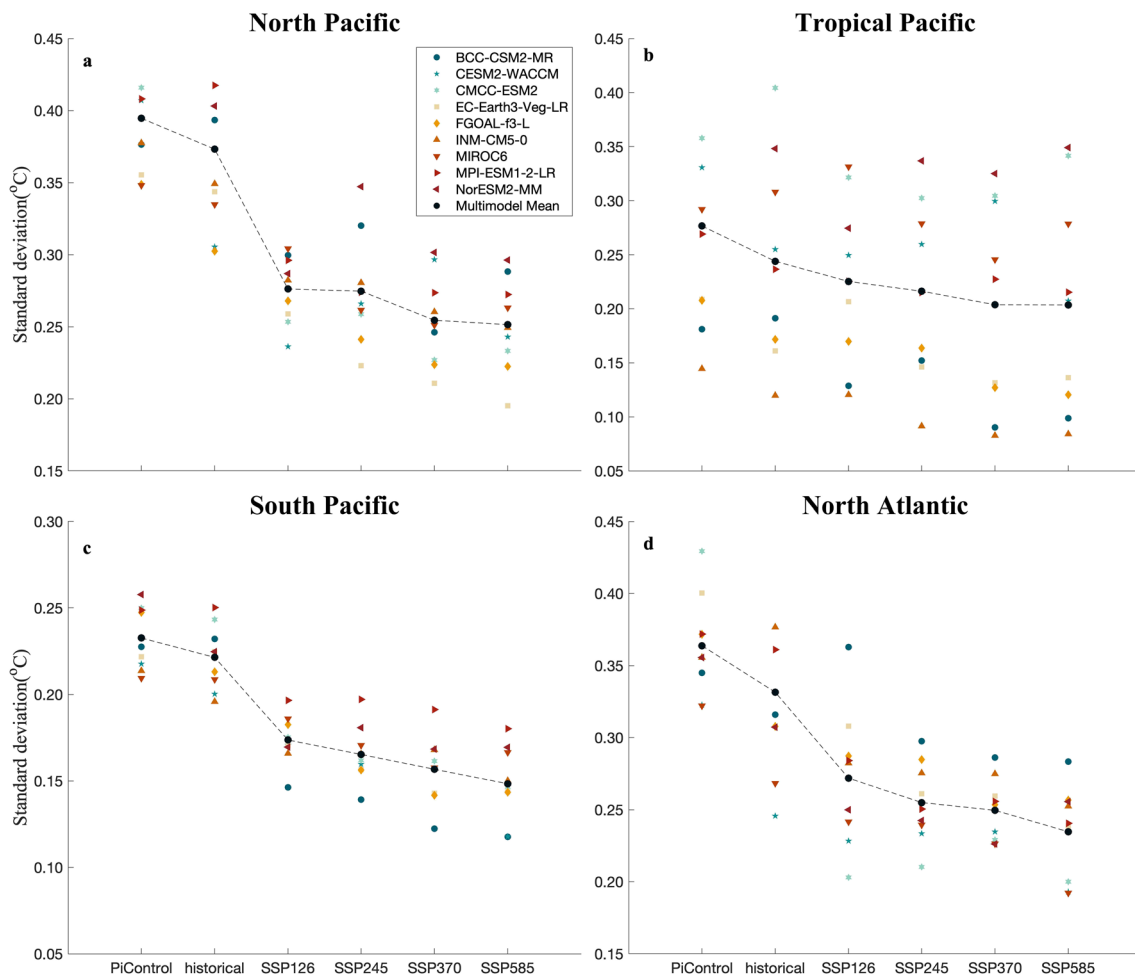


**Fig. 3** The change of SST standard deviation in the **a** NP, **b** TP, and **c** SP, and **d** NA. After removing the long-term trend and using a 3-year running mean twice, the standard deviation of yearly data was calculated at each point, and then the regional average was calculated.

Nine dots in different colors represent nine CMIP6 models, and black represents multi-model mean. Combining black dots from PI to different global warming scenarios shows the trends of amplitude in the four regions

model members, which is double the size compared to the relevant previous studies (Cheng et al. 2016; Wu and Liu 2020). The shortening of the period for all four indices is also featured in most models used here (Figs. S7–S10). For the PDO period (Fig. 4a), the peaks of the PI are approximately 40 years, and this peak in the HIS becomes weaker, and the 30-year peak becomes more dominant. Under different global warming scenarios, the peaks tend to shift to shorter periods. Similarly, reductions in the period can also be seen in the SPDO and AMV. These results are still valid when using more models in CMIP6 (13 models, not shown). Two points need to be mentioned based on the power spectra of the four indices. First, the low-frequency power is weak for the TPDV PI and HIS simulations compared to the global warming scenarios (Fig. 4b), and the power shifts to high frequency when the temperature rises. Second is that the AMV only has a period of less than 50 years in future

scenarios because of the data length (Table 1). This creates a discrepancy with the observation which has a 70-year period and has no signal in 35-year (Fig. 11). It is worth mentioning that statistical confidence for decadal variability under the warming scenarios would be lower than during the PI, which is longer than the HIS and SSPs, especially then considering multi-decadal variability. Longer time series simulation data are desired to verify the multidecadal response in the future.

In summary, the analysis above on the ensemble of the nine CMIP6 models suggests that all decadal variabilities become weaker due to shorter periods under different strengths of global warming, although the patterns are still similar to the PI condition. Specifically, the response of the TPDV is relatively modest compared to the other indices, which might represent the weaker temperature response in the tropical regions as compared to the response at higher latitudes.

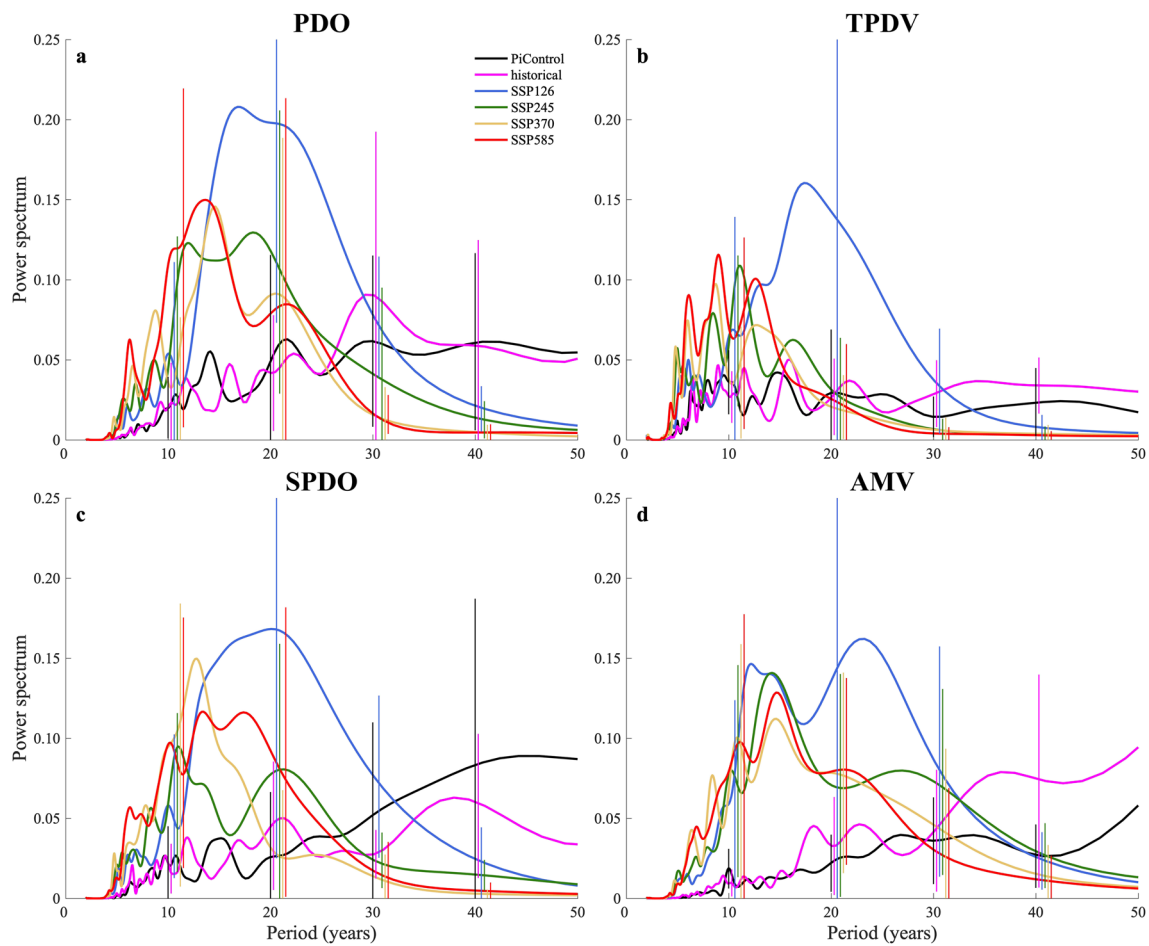


**Fig. 4** Multi-model mean power spectra of **a** PDO, **b** TPDV, **c** SPDO, and **d** AMV from the simulations of the PI, HIS, and four projected global warming scenarios (SSP1-2.6, SSP2-4.5, SSP3-7.0, and SSP5-8.5) by nine CMIP6 models. The linear warming trend has been

removed before calculating decadal variability and the power spectrum of each model has been normalized at first. The vertical lines over each power spectrum indicate cross-model standard deviation

**Table 2** The main periods of PDO, TPDV, SPDO, and AMV from the simulations of the PI, HIS, and four global warming scenarios (SSP1-2.6, SSP2-4.5, SSP3-7.0, and SSP5-8.5) by nine CMIP6 multi-model mean

	Indices	Pre-industrial runs (year)	Historical runs (year)	SSP1-2.6 runs (year)	SSP2-4.5 runs (year)	SSP3-7.0 runs (year)	SSP5-8.5 runs (year)
1	PDO	40	30	20	20	15	13
2	TPDV	15	15	20	15	10	10
3	SPDO	45	36	20	20	13	15
4	AMV	36	36	25	15	15	15

### 4 Conclusions and discussion

A systematic study on the response of ocean decadal variability to global warming is performed for the North Pacific, Tropical Pacific, South Pacific, and North Atlantic using nine CMIP6 models under four global warming scenarios. The observed decadal variability shows that the PDO has bi-decadal and multidecadal signals, and the

TPDV and SPDO only have periods of approximately 20 to 30 years while the AMV has a strong 70-year period. These four decadal variabilities have periods of approximately 30–40 years in CMIP6 models and have a robust spectral power shift from low frequency toward high frequency, which is clear in wavelet analysis (Fig. S17). The CMIP6 models can reproduce reasonable PDO, TPDV, SPDO, and AMV in the PI and HIS simulations, with the

patterns changing little under the global warming scenarios. It is notable that the amplitudes become weaker with warmer background temperatures, which is robust within all decadal variabilities and is consistent with previous findings (Wang and Li 2017; Li et al. 2020). The weakening of the NP and NA is approximately 40% from the PI to SSP5-8.5 simulations in the CMIP6 modes, which is close to that seen in the CMIP5 models (37%) (Wu and Liu 2020). It is worth noting that the multimodel mean of the TP has a 30% decrease under global warming, although some models (e.g., NorESM2-MM) show a different trend from the perspective of the model average. Previous studies imply that this weakening in the decadal variabilities is caused partly by the weakened atmospheric stochastic forcing and the increased SST damping rate (Wu and Liu 2020). This result is established in the mid-high latitudes, and the tropical atmosphere forcing seems to change little under global warming (Fig. S15e–h). The shortened period is caused by the acceleration of ocean Rossby waves (Fang et al. 2014) which is also different in the equatorial regions.

Overall, under global warming, the shortening and weakening of the decadal variabilities are both robust across the global regions in CMIP6 models. And the shortening of periods is also established in the CESM large ensemble with longer data length (180 years) (Fig. S16). However, the TPDV has a weaker response which might be related to the tropical atmospheric forcing. And the pattern of the decadal variabilities will not change in the future, which suggests the dynamical process may not change under global warming. However, the expression outside the chosen regions of each decadal variability is weakened in the future scenarios (Figs. S1–4), which could be related to the change of teleconnection between different regions or the industrial aerosols or greenhouse gases forcing signal in decadal variabilities indices (Baek et al. 2022). In this study, we provide an overview of the responses of global ocean decadal variability in the future. Further studies are needed to verify these results by using longer data and understanding the mechanism in different regions.

**Supplementary Information** The online version contains supplementary material available at <https://doi.org/10.1007/s10236-023-01590-8>.

**Funding** This work is supported by the National Natural Science Foundation of China under Grant 42105043, and Chinese MOST (2017YFA0603801). The analyses are performed on the Marine Big Data Center of Institute for Advanced Ocean Study of Ocean University of China and High-performance Computing Platform of Peking University. This work is also supported by Postdoctoral Innovation Project of Shandong Province.

**Data availability** The ERSST dataset is downloaded from <https://www.ncei.noaa.gov/products/extended-reconstructed-sst>. The CMIP6 dataset is downloaded from <https://esgf-node.llnl.gov/search/cmip6/>. The

datasets generated during and/or analyzed during the current study are available from the corresponding author on reasonable request.

## Declarations

**Competing interests** The authors declare no competing interests.

**Open Access** This article is licensed under a Creative Commons Attribution 4.0 International License, which permits use, sharing, adaptation, distribution and reproduction in any medium or format, as long as you give appropriate credit to the original author(s) and the source, provide a link to the Creative Commons licence, and indicate if changes were made. The images or other third party material in this article are included in the article's Creative Commons licence, unless indicated otherwise in a credit line to the material. If material is not included in the article's Creative Commons licence and your intended use is not permitted by statutory regulation or exceeds the permitted use, you will need to obtain permission directly from the copyright holder. To view a copy of this licence, visit <http://creativecommons.org/licenses/by/4.0/>.

## References

- Alexander M (2010) Extratropical air–sea interaction, sea surface temperature variability, and the Pacific decadal oscillation. *Clim Dyn* 123:148
- Baek SH, Kushnir Y, Ting M, Smerdon JE, Lora JM (2022) Regional signatures of forced north atlantic sst variability: a limited role for aerosols and greenhouse gases. *Geophys Res Lett* 49(8):e2022GL097794
- Bordbar MH, Martin T, Latif M, Park W (2017) Role of internal variability in recent decadal to multidecadal tropical Pacific climate changes. *Geophys Res Lett* 44:4246–4255
- Bordbar MH, England MH, Sen Gupta A, Santoso A, Taschetto AS, Martin T, Park W, Latif M (2019) Uncertainty in near-term global surface warming linked to tropical Pacific climate variability. *Nat Commun* 10:1990
- Cheng J, Liu Z, Zhang S, Liu W, Dong L, Liu P, Li H (2016) Reduced interdecadal variability of Atlantic meridional overturning circulation under global warming. *Proc Natl Acad Sci* 113(12):3175–3178
- Chu P-S, Clark JD (1999) Decadal variations of tropical cyclone activity over the central North Pacific. *Bull Am Meteor Soc* 80(9):1875–1882
- Clement A, Bellomo K, Murphy LN, Cane MA, Mauritsen T, Rädel G, Stevens B (2015) The Atlantic multidecadal oscillation without a role for ocean circulation. *Science* 350(6258):320–324
- Deser C, Blackmon ML (1993) Surface climate variations over the North Atlantic Ocean during winter: 1900–1989. *J Clim* 6(9):1743–1753
- Deser C, Alexander MA, Xie S-P, Phillips AS (2010) Sea surface temperature variability: patterns and mechanisms. *Annu Rev Mar Sci* 2(1):115–143
- Deser C, Guo R, Lehner F (2017) The relative contributions of tropical Pacific sea surface temperatures and atmospheric internal variability to the recent global warming hiatus. *Geophys Res Lett* 44(15):7945–7954
- Di Lorenzo E, Mantua N (2016) Multi-year persistence of the 2014/15 North Pacific marine heatwave. *Nat Clim Chang* 6(11):1042–1047
- Di Lorenzo E, Schneider N, Cobb KM, Franks P, Chhak K, Miller AJ, McWilliams JC, Bograd SJ, Arango H, Curchitser E (2008) North Pacific gyre oscillation links ocean climate and ecosystem change. *Geophys Res Lett* 35:L08607
- Di Lorenzo E, Xu T, Zhao Y, Newman M, Capotondi A, Stevenson S, Amaya D, Anderson B, Ding R, Furtado J (2023) Modes and



- mechanisms of Pacific decadal-scale variability. *Ann Rev Mar Sci* 15:249–275
- Ding H, Greatbatch RJ, Latif M, Park W, Gerdes R (2013) Hindcast of the 1976/77 and 1998/99 climate shifts in the Pacific. *J Clim* 26(19):7650–7661
- Ding H, Newman M, Alexander MA, Wittenberg AT (2019) Diagnosing secular variations in retrospective ENSO seasonal forecast skill using CMIP5 model-analogs. *Geophys Res Lett* 46(3):1721–1730
- Enfield DB, Mestas-Nuñez AM, Trimble PJ (2001) The Atlantic multidecadal oscillation and its relation to rainfall and river flows in the continental US. *Geophys Res Lett* 28(10):2077–2080
- England MH, McGregor S, Spence P, Meehl GA, Timmermann A, Cai W, Gupta AS, McPhaden MJ, Purich A, Santoso A (2014) Recent intensification of wind-driven circulation in the Pacific and the ongoing warming hiatus. *Nat Clim Chang* 4(3):222–227
- England MH, Kajtar JB, Maher N (2015) Robust warming projections despite the recent hiatus. *Nat Clim Chang* 5:394–396
- Fang C, Wu L, Zhang X (2014) The impact of global warming on the Pacific decadal oscillation and the possible mechanism. *Adv Atmos Sci* 31(1):118–130
- Farneti R (2017) Modelling interdecadal climate variability and the role of the ocean. *Wiley Interdisc Rev* 8(1):e441
- Flandrin P, Rilling G, Goncalves P (2004) Empirical mode decomposition as a filter bank. *IEEE Sign Process Lett* 11(2):112–114
- Hare SR, Mantua NJ, Francis RC (1999) Inverse production regimes: Alaska and west coast Pacific salmon. *Fisheries* 24(1):6–14
- Hawkins E, Sutton R (2009) The potential to narrow uncertainty in regional climate predictions. *Bull Am Meteor Soc* 90(8):1095–1108
- Holbrook NJ, Scannell HA, Sen Gupta A, Benthuyens JA, Feng M, Oliver EC, Alexander LV, Burrows MT, Donat MG, Hobday AJ (2019) A global assessment of marine heatwaves and their drivers. *Nat Commun* 10(1):1–13
- Hsu HH, Chen YL (2011) Decadal to bi-decadal rainfall variation in the western Pacific: a footprint of South Pacific decadal variability? *Geophys Res Lett* 38:L03703
- Huang B, Banzon VF, Freeman E, Lawrimore J, Liu W, Peterson TC, Smith TM, Thorne PW, Woodruff SD, Zhang H-M (2015) Extended reconstructed sea surface temperature version 4 (ERSST.v4). Part I: upgrades and intercomparisons. *J Clim* 28(3):911–930
- Huang J, Xie Y, Guan X, Li D, Ji F (2017) The dynamics of the warming hiatus over the Northern Hemisphere. *Clim Dyn* 48(1):429–446
- IPCC (2013) *Climate Change 2013: the Physical Science Basis. Working Group I Contribution to the Fifth Assessment of the Intergovernmental Panel on Climate Change*. Cambridge University Press, Cambridge and New York
- Joyce TM, Zhang R (2010) On the path of the Gulf Stream and the Atlantic meridional overturning circulation. *J Clim* 23(11):3146–3154
- Kosaka Y, Xie S-P (2013) Recent global-warming hiatus tied to equatorial Pacific surface cooling. *Nature* 501(7467):403–407
- Kushnir Y (1994) Interdecadal variations in North Atlantic sea surface temperature and associated atmospheric conditions. *J Clim* 7(1):141–157
- Li D (2022) Physical processes and feedbacks obscuring the future of the Antarctic Ice Sheet. *Geosystems and Geoenvironment* 1(4):100084
- Li W, Li L, Deng Y (2015) Impact of the interdecadal Pacific oscillation on tropical cyclone activity in the North Atlantic and eastern North Pacific. *Sci Rep* 5(1):1–8
- Li S, Wu L, Yang Y, Geng T, Cai W, Gan B, Chen Z, Jing Z, Wang G, Ma X (2020) The Pacific decadal oscillation less predictable under greenhouse warming. *Nat Clim Chang* 10(1):30–34
- Liu Z (2012) Dynamics of interdecadal climate variability: a historical perspective. *J Clim* 25(6):1963–1995
- Liu Z, Di Lorenzo E (2018) Mechanisms and predictability of Pacific decadal variability. *Curr Clim Chang Rep* 4(2):128–144
- Liu W, Huang B, Thorne PW, Banzon VF, Zhang H-M, Freeman E, Lawrimore J, Peterson TC, Smith TM, Woodruff SD (2015) Extended reconstructed sea surface temperature version 4 (ERSST.v4): Part II. Parametric and structural uncertainty estimations. *J Clim* 28(3):931–951
- Mantua NJ, Hare SR, Zhang Y, Wallace JM, Francis RC (1997) A Pacific interdecadal climate oscillation with impacts on salmon production. *Bull Am Meteor Soc* 78(6):1069–1080
- McGregor S, Timmermann A, Stuecker MF, England MH, Merrifield M, Jin F-F, Chikamoto Y (2014) Recent walker circulation strengthening and Pacific cooling amplified by Atlantic warming. *Nat Clim Chang* 4(10):888–892
- Newman M, Alexander MA, Ault TR, Cobb KM, Deser C, Di Lorenzo E, Mantua NJ, Miller AJ, Minobe S, Nakamura H (2016) The Pacific decadal oscillation, revisited. *J Clim* 29(12):4399–4427
- O’Neill BC, Tebaldi C, Van Vuuren DP, Eyring V, Friedlingstein P, Hurtt G, Knutti R, Kriegler E, Lamarque J-F, Lowe J (2016) The scenario model intercomparison project (ScenarioMIP) for CMIP6. *Geosci Model Dev* 9(9):3461–3482
- Power S, Casey T, Folland C, Colman A, Mehta V (1999) Inter-decadal modulation of the impact of ENSO on Australia. *Clim Dyn* 15(5):319–324
- Roemmich D, McGowan J (1995) Climatic warming and the decline of zooplankton in the California current. *Science* 267(5202):1324–1326
- Shakun JD, Shaman J (2009) Tropical origins of North and South Pacific decadal variability. *Geophys Res Lett* 36:L19711
- Smith TM, Reynolds RW, Peterson TC, Lawrimore J (2008) Improvements to NOAA’s historical merged land–ocean surface temperature analysis (1880–2006). *J Clim* 21(10):2283–2296
- Song YH, Chung E-S, Shahid S (2022) Uncertainties in evapotranspiration projections associated with estimation methods and CMIP6 GCMs for South Korea. *Sci Total Environ* 825:153953
- Taylor KE (2001) Summarizing multiple aspects of model performance in a single diagram. *J Geophys Res* 106(D7):7183–7192
- Thapliyal A, Kimothi S, Taloor AK, Bisht MP, Mehta P, Kothiyari GC (2023) Glacier retreat analysis in the context of climate change impact over the Satopanth (SPG) and Bhagirathi-Kharak (BKG) glaciers in the Mana basin of the Central Himalaya, India: A geospatial approach. *Geosystems and Geoenvironment* 2(1):100128
- Wang J, Li C (2017) Low-frequency variability and possible changes in the North Pacific simulated by CMIP5 models. *J Meteorol Soc Japan Ser II* 95:199
- Wu S, Liu Z-Y (2020) Decadal variability in the North Pacific and North Atlantic under global warming: the weakening response and its mechanism. *J Clim* 33(21):9181–9193
- Wu S, Liu Z-Y, Cheng J, Li C (2018) Response of North Pacific and North Atlantic decadal variability to weak global warming. *Adv Clim Chang Res* 9(2):95–101
- Wu S, Liu Z, Du J, Liu Y (2022) Change of global ocean temperature and decadal variability under 1.5° C warming in FOAM. *J Mar Sci Eng* 10(9):1231
- Zhang Y, Wallace JM, Battisti DS (1997) ENSO-like interdecadal variability: 1900–93. *J Clim* 10(5):1004–1020
- Zhang R, Sutton R, Danabasoglu G, Delworth TL, Kim WM, Robson J, Yeager SG (2016) Comment on “The Atlantic multidecadal oscillation without a role for ocean circulation.” *Science* 352(6293):1527–1527
- Zhang R, Sutton R, Danabasoglu G, Kwon YO, Marsh R, Yeager SG, Amrhein DE, Little CM (2019) A review of the role of the Atlantic meridional overturning circulation in Atlantic multidecadal variability and associated climate impacts. *Rev Geophys* 57(2):316–375